Creation of high-energy phonons in superfluid ^{4}He and the dependence of their angular distribution on heater size

D. H. S. Smith and A. F. G. Wyatt*
School of Physics, University of Exeter, Exeter EX4 4QL, United Kingdom
(Received 1 February 2010; revised manuscript received 15 March 2010; published 16 April 2010)

The angular distributions of high-energy phonons, that are created by a short pulse of low-energy phonons propagating in superfluid ^{4}He, are measured for different heater sizes and heater powers. We find that the intrinsic full width at half height of the high-energy phonons is proportional to the reciprocal of the width of the heater that creates the low-energy phonons. This is similar to the behavior shown by the low-energy phonons where the width of the phonon sheet is inversely proportional to the heater width. We discuss the correspondence between the formation of the phonon sheet by the low-energy phonons and the creation of high-energy phonons, and conclude that the phonon sheet is caused by the creation of high-energy phonons within a few millimeters of the heater. We also show that the total energy in the high-energy phonons increases linearly with heater power, once a threshold power is reached. This indicates that the initial low-energy phonons increase in number but not energy, as the heater power is increased.

DOI: 10.1103/PhysRevB.81.134519 PACS number(s): 67.10.−j

I. INTRODUCTION

That high-energy phonons can be copiously created from low-energy phonons is one of the amazing properties of phonon pulses propagating in superfluid ^{4}He.[1–4] A phonon pulse is an example, indeed an extreme example, of an anisotropic phonon system and, over the last decade, we have shown that anisotropic phonon systems have very different behavior to the usual isotropic ones, see Ref. 5, and references therein. In this paper, we investigate how the creation of high-energy phonons depends on the size of the heater that creates the pulse of low-energy phonons and we shall relate the creation of high-energy phonons to the formation of a mesa-shaped angular distribution of the low-energy phonons.[6,7] High-energy phonons, or *h*-phonons, have an energy of 10 K and just above, at the saturated vapor pressure at $T \leq 1$ K. Low-energy phonons, or *l*-phonons, have energies <2 K depending on the energy density in the *l*-phonon system. These two groups of phonons are indicated in Fig. 1(a), and in Fig. 1(b) we show the *l*-phonons separated in time from the *h*-phonons by dispersion.

An anisotropic system is one in which there is a relative velocity between the normal fluid and the superfluid. Such systems have been created in such classic flow experiments as Allen and Misener,[8] Kapitza,[9] and Craig and Pellam.[10] In those systems, the normal fluid is stationary and the superfluid moves with a low velocity relative to the Landau critical velocity. In this paper, the pulse of low-energy phonons is a strongly interacting phonon system, and these phonons constitute the normal fluid that moves through the superfluid at a high relative velocity. These low-energy phonons are in a quasiequilibrium by which we mean an equilibrium that slowly changes on the time scale of the experiment.[11]

The pulse of low-energy phonons, or equivalently a small volume of normal fluid, moves through the superfluid with a velocity almost exactly equal to the sound velocity.[12] This is the maximum velocity that a normal fluid of only phonons can have,[13–16] and it is much higher than the usual critical velocity for a normal fluid with rotons, i.e., the Landau critical velocity. The superfluid is very nearly stationary with respect to the experimental cell. The normal fluid can be described by two variables, a thermodynamic temperature and a velocity, instead of only one variable, temperature, for the isotropic system. This velocity is the relative velocity between the normal fluid and the superfluid, which to a very good approximation is the velocity of the phonon pulse relative to the experimental cell. The phonon number density is low and so the density of the normal fluid ρ_n is very small relative to the total density ρ so $\rho_n \ll \rho_s \sim \rho$, where ρ_s is the density of the superfluid and $\rho_n + \rho_s = \rho$. Correspondingly, the quasiequilibrium temperature T of the phonons is very low compared to the Lambda temperature where $\rho_n = \rho$. Typically, $T \sim 0.04$ K and the relative velocity is 0.98 c, where c is the velocity of sound in liquid helium.

The distribution of the momenta of the low-energy phonons in the pulse is strongly anisotropic. In momentum space, there is approximately an occupied cone of momentum states with the cone axis in the direction of the velocity of the pulse. The cone angle is given by the temperature and relative velocity. It is narrow, typically less than 10°. We can imagine this cone cut from an isotropic momentum distribution characterized by a temperature T_p. This intuitive picture

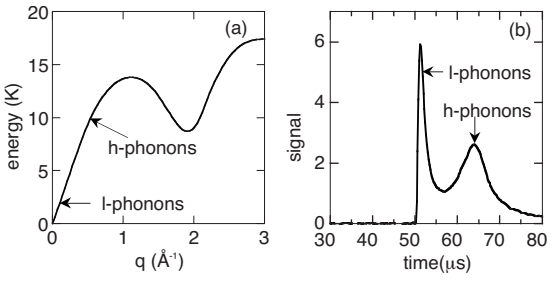

FIG. 1. (a) shows the dispersion curve for phonons and rotons in ^{4}He at the saturated vapor pressure at $T < 1$ K. The positions of the low (l) and high (h) energy phonons are indicated. (b) shows a typical phonon signal as a function of time from the start of the heater pulse, at $\theta = 0$. The first peak is from the *l*-phonons and the broader second peak is due to *h*-phonons as indicated.

of an anisotropic phonon distribution is called the Bose-cone approximation. T_p is typically ≤ 1 K. The relation between the Bose-cone approximation and the exact quasiequilibrium is given in Refs. 17 and 18. We note that $T_p \gg T$.

The low-energy phonons in the pulse strongly interact by the three-phonon process (3pp) scattering.[17,19] In this scattering, phonon number is not conserved as one phonon goes to two phonons and vice versa, and energy and momentum are conserved. The 3pp scattering rate is very high on the scale of the inverse time for phonon propagation in the experiment. There is also a much slower scattering by the four-phonon process, 4pp.[20,21] This process does conserve phonon number as two phonons scatter to give two new phonons, again, with energy and momentum conserved. It is the 4pp scattering which creates the high-energy phonons while the 3pp scattering maintains the quasiequilibrium between the low-energy phonons. The creation of high-energy phonons causes a relatively rapid loss of energy from the low-energy phonon system. The high-energy phonons are lost from the low-energy pulse because they have a lower group velocity than the low-energy phonons. As the high-energy phonons escape more readily from a pulse of small spatial extent along the propagation direction, a short pulse is necessary for a large conversion of the initial energy into high-energy phonons. In a long pulse, the high-energy phonons do not readily escape and so they form a suprathermal density within the low-energy phonon pulse.[22]

For many years, it was thought that 3pp could not happen in liquid ^{4}He, see, for example, Ref. 23. This idea followed from the erroneous belief that the dispersion curve for phonons was slightly below linear. That is, $\omega = cq(1-aq^2)$, where a is a positive coefficient. However, the phonon attenuation in liquid ^{4}He, at zero pressure, could only be explained if 3pp were possible.[24,25] This was confirmed experimentally by showing that a beam of phonons spread out in angle due to 3pp decays, at zero pressure but not at high pressures.[26] So actually a is a negative coefficient and the dispersion is described as anomalous at low pressure. The anomalous dispersion ceases at high momenta; at zero pressure, it is anomalous in the range $0 < q < q_c$, where $q_c = 0.55$ Å.[27,28] The corresponding energy is $\hbar q_c / k_B = 10$ K. As pressure is increased, q_c decreases and goes to zero at a pressure of 19 bar.[26–28]

The angular distribution of the l-phonons showed a surprising shape at zero pressure.[6] At small angles to the normal to the heater, the energy flux in the l-phonons was independent of angle. This means that the l-phonons form a propagating phonon sheet in the liquid helium in which the aerial energy density of the l-phonons is uniform and outside of this sheet, the energy density falls away, i.e., when the angle reached a certain small value, the energy flux decreased rapidly with increasing angle. So in a plot of energy flux versus angle, the curve showed a mesa shape, i.e., a flat top with steeply falling sides. The top of the mesa is the phonon sheet. Recently it was shown that the angular width of the mesa top, or equivalently the phonon sheet, was related to the size of the heater; the angular width of the mesa was inversely proportional to the heater width.[7]

In the first paper on the mesa,[6] it was proposed that the mesa shape was related to the creation of high-energy phonons: Immediately after the heater pulse, the low-energy phonons have an angular distribution of energy which is highest along the direction normal to the heater and decreases as the angle to the normal increased. As the h-phonon creation rate is a strong function of energy density,[29] broadly speaking, above a certain energy density ε_h, there is increasing h-phonon creation and below it, little h-phonon creation. So h-phonons are created in directions near to the heater normal. When h-phonons are created, the energy density of the l-phonons decreases and so h-phonons will continue to be created until the l-phonon energy density ε_h is reached. We identify the mesa top with the lateral extent of the l-phonon system which has reached an energy density ε_h. The steep sides of the mesa are due to phonons that are outside of the strongly interacting core of the l-phonons and so have decayed in phonon energy. Their lower-energy density and the lower sensitivity of the detector to lower-energy phonons,[30] means that the signal drops rapidly with increasing angle.

In the second mesa paper,[7] these ideas were developed. The central idea is that the 3pp interaction rate between the l-phonons depends on their energy density, and this is initially determined by the angle of emission from the heater. The angular dependence of the emission from the heater is obtained from measurements at a pressure of 24 bar and 50 mK,[31] where the injected phonons do not scatter or decay. At this pressure, the angular distribution, at distances large compared with the dimensions of the heater, varies as $\cos(\theta)$ which means that each point on the heater radiates isotropically into the liquid helium. As the angle to the heater normal increases from zero, the energy density decreases because the extent of the pulse increases in the direction of propagation of the pulse. This length varies as $h \sin(\theta) + ct_p$, where h is the width of the heater and t_p is the pulse length. Unless the angle θ is very small, $h \sin(\theta) > ct_p$ and the energy density is $\propto \cos(\theta)/h \sin(\theta)$. Now at zero pressure, if the energy density is high enough, the l-phonons are in a quasiequilibrium with a balance between phonon scattering that increases and decreases the phonon energies. In the other extreme, if the density is very low in an elemental volume, the phonons in that volume only decay in energy by 3pp. At intermediate densities, which occur at intermediate angles, the phonon scattering that decreases phonon energy, dominates scattering that increases phonon energy so that there is a continual decrease in phonon energies as the pulse propagates. This decreases the signal, due to the energy sensitivity of the detector, even though the energy flux remains nearly constant (see Fig. 4 in Ref. 7). Only in the regions of high-energy density are h-phonons created, that is at small angles to the heater normal.

This model[7] showed that the full angular width of the mesa, $2\theta_A$, is given by

$$\tan(\theta_A) = \frac{ct_p}{0.4fh}, \tag{1}$$

where $f \sim 1$. Note that θ_A is only weakly dependent on heater power; the only dependence is through the factor f. We see that the width of the mesa should be inversely proportional to the width of the heater. This dependence was found experimentally.[7]

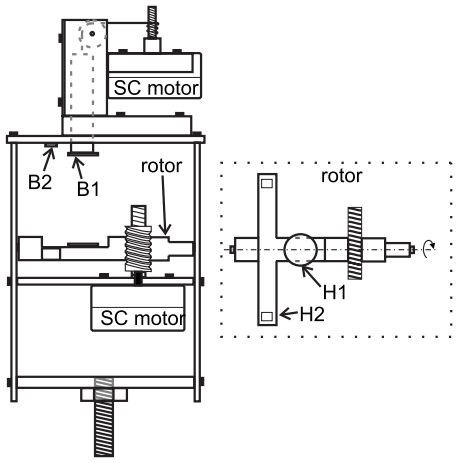

FIG. 2. Diagram of the apparatus. The arrow H1 points to the substrate for the three heaters of different widths. The central heater is the 1×1 mm^2 heater which is opposite the main bolometer B1. H2 and B2 are the heater and bolometer for the measurements of the angle. The heater substrates are mounted on a rotor driven by a superconducting stepping motor. The separation of the central heaters and the main bolometer is controlled by a second stepping motor.

The model also couples the formation of the mesa in the *l*-phonon angular distribution with the creation of *h*-phonons. So it predicts that the angular width of the angular distribution of *h*-phonons should depend on the heater width, in a similar or related way to the mesa dependence on heater width.

There is another model for the later development of the mesa that does not involve any *h*-phonons[32] and so applies after the period of intense *h*-phonon creation. The model only involves the behavior of a cool low-energy phonon beam where there are no *h*-phonons, which is after the pulse has propagated a few millimeters from the heater. So this model does not apply to the behavior of the *h*-phonons. The initial state for the model is envisioned as a slab of helium occupied by low-energy phonons and bounded by a phonon vacuum. In this model, the mesa width is increased by a second-sound wave in the *l*-phonon system.

In this paper, we report measurements of the angular distribution of *h*-phonons from different sized heaters and at different heater powers. We shall see that the full width at half height, FWHH, of the *h*-phonon angular distribution is larger for a smaller width heater. We shall argue that this is strong evidence for the *h*-phonon creation process causing the angular distribution of the *l*-phonons to form a mesa shape within a few millimeters of the heater.

The paper is organized as follows. The experiment is described in Sec. II, and in Sec. III, the results are presented. In Sec. IV, the results are analyzed and discussed and conclusions are drawn in Sec. V.

II. EXPERIMENTAL METHOD AND APPARATUS

The experimental arrangement is shown in Fig. 2, it is the same arrangement as used in Ref. 7. A substrate with three thin-film gold heaters is mounted on the axis of a holder with radial arms. The holder can be rotated by a stepping motor which drives through a worm gear. The angle θ of the rotor is measured by timing phonon pulses from the heaters mounted at the ends of the radial arms, to fixed detectors which are $\sim$20 mm above them. In this way, we obtain an angular accuracy of $\sim0.3°$. The main detector is mounted on the end of a vertical bar which is directly above the heater. This bar can move vertically and is driven by a second stepping motor through a cotton thread connection. The cross section of the bar is square, and the bar moves through a square sectioned guide channel so that its end is laterally positioned. The distance between the central 1×1 mm^2 heater and the bolometer is found from the time of flight of low-energy phonons.

Three thin-film gold heaters were evaporated onto a polished sapphire substrate 7.5 mm diameter and 0.4 mm thick. The heater dimensions were 0.25×1 mm^2, 1×1 mm^2, and 0.5×1 mm^2. The rotation axis passed through the center of the 1×1 mm^2 heater. The long directions of the other two heaters were parallel to the rotation axis. As phonons propagate ballistically in sapphire, the opposite side of the sapphire disk was deliberately roughened so that it would diffusely reflect the phonons injected into the substrate and so distribute them over all angles. This means that very few of these phonons go into the liquid helium near the heater. In earlier experiments with glass substrates, there had been a low level but long tail to the detected phonon signal which came from phonons diffusing out of the glass substrate. With a sapphire substrate, there is a well-defined single phonon pulse injected into the liquid helium and no thermal tail in the detected signal.

The detector was a zinc film, $\sim$100 nm thick, evaporated onto a very thin matching layer of silver on a polished sapphire substrate 10 mm diameter and 1 mm thick. The zinc film was scratched into a serpentine track over an area of 1×1 mm^2. A superconducting solenoid gave a magnetic field that held the zinc near its superconducting transition boundary. The bolometer was in a bridge with electronic feedback that maintained it at a constant resistance and, hence, temperature of ~0.35 K.[33–35] Recent experiments have shown that the sensitive area of the bolometer is actually only ~0.1 mm$\times\sim0.1$ mm.[36] It is most likely that the sensitive region is a single superconducting-normal boundary across the track width of ~0.1 mm.

The apparatus was sealed in a brass cell that was filled with ultrapure liquid ^{4}He (Ref. 37) and could be pressurized up to 24 bar. The pressure was measured with a Budenberg Standard Test Gauge to an accuracy of 0.02 bar. The cell was mounted on a dilution refrigerator which maintained the temperature of the cell at $\sim$50 mK during measurements.

The heater was pulsed by a Le Croy 9210 pulse generator at various powers in the range 3–25 mW, with a repetition rate of 45 Hz. The signal was amplified with an EG and G 5113 preamplifier, and captured and averaged in a Tectronix DSA 601A to increase the signal-to-noise ratio. The bolometer signal as a function of time shows two sets of phonons, a typical signal is shown in the inset of Fig. 1(b); the low-energy phonons travel at the velocity of sound and have little dispersion and the high-energy phonons, which arrive later, have a relatively large dispersion. The *h*-phonons start at the

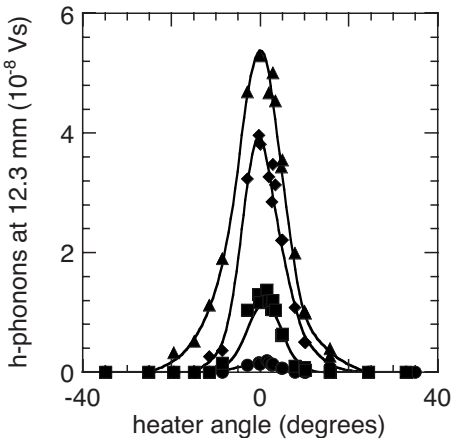

FIG. 3. The angular distribution of the time-integrated *h*-phonon signal for the 1 mm × 1 mm heater, at a heater-bolometer separation of 12.3 mm, for heater powers 3.125 mW (circles), 6.25 mW (squares), 12.5 mW (diamonds), and 25 mW (triangles). The heater pulse is 100 ns and the pressure 0 bar.

beginning of the *l*-phonons so there is some overlap between the two signals. The *h*-phonon signal has to be extrapolated by hand to its start under the *l*-phonon signal. This involves ~5% of the *h*-phonon signal and so creates an uncertainty of ~1% in the final time-integrated signal. In what follows, the term *h*-phonon signal will mean the total *h*-phonon signal integrated over time. It gives a measure of the *h*-phonons with the least uncertainty.

III. EXPERIMENTAL RESULTS

In Figs. 3–6, we show the angular distribution of the *h*-phonon signal from two heaters at two heater-bolometer distances for different heater powers. We shall refer to the 1×1 mm^2 and 0.25×1 mm^2 heaters heater as the 1 mm and 0.25 mm heaters, respectively, and the heater-bolometer distances as 12.3 and 8.2 mm. Figures 3–6 are, respectively,

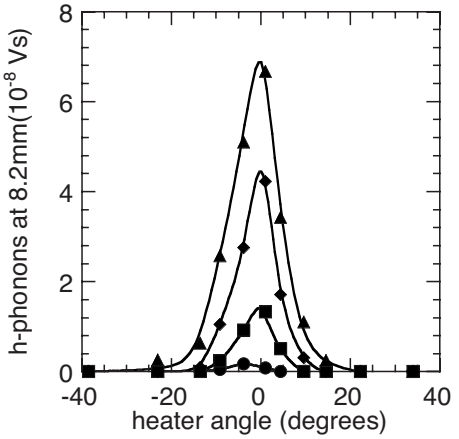

FIG. 4. The angular distribution of the time-integrated *h*-phonon signal for the 1 mm × 1 mm heater, at a heater-bolometer separation of 8.2 mm, for heater powers 3.125 mW (circles), 6.25 mW (squares), 12.5 mW (diamonds), and 25 mW (triangles). The heater pulse is 100 ns and the pressure 0 bar.

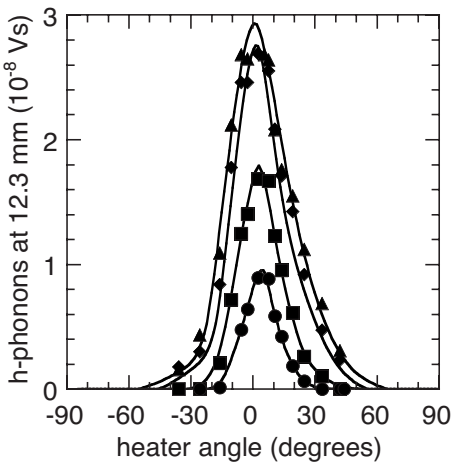

FIG. 5. The angular distribution of the time-integrated *h*-phonon signal for the 0.25 mm × 1 mm heater, at a heater-bolometer separation of 12.3 mm, for heater powers 3.125 mW (circles), 6.25 mW (squares), 12.5 mW (diamonds), and 25 mW (triangles). The heater pulse is 100 ns and the pressure 0 bar. Note that the angular distribution is much wider than for the 1 mm × 1 mm heater shown in Fig. 3.

for the heater and distance combinations, 1, 12.3; 1, 8.2; 0.25, 12.3; and 0.25, 8.2. We see immediately that the angular distributions are narrow and similar for the same heater but differ considerably between heaters. The narrower distributions come from the wider heater. We also see that there is only a very small signal for the 3.125 mW heater pulses from the 1 mm heater whereas there is a relatively large signal from this power with the 0.25 mm heater. Clearly the heater power per unit area of heater is the important factor in creating *h*-phonons, and we will see later that there is a threshold heater power density for creating *h*-phonons.

In Fig. 7, the full widths at half height, FWHH, of the angular distributions shown in Figs. 3–6, are shown as a

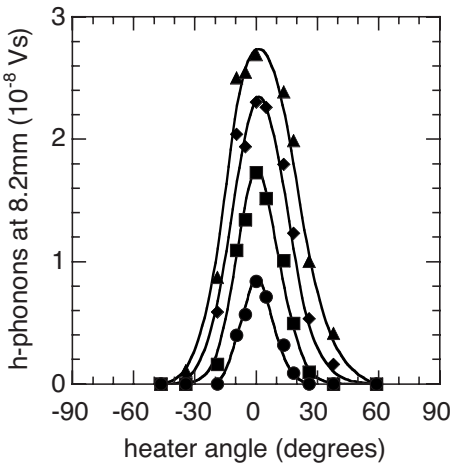

FIG. 6. The angular distribution of the time-integrated *h*-phonon signal for the 0.25 mm × 1 mm heater, at a heater-bolometer separation of 8.2 mm, for heater powers 3.125 mW (circles), 6.25 mW (squares), 12.5 mW (diamonds), and 25 mW (triangles). The heater pulse is 100 ns and the pressure 0 bar. Note that the angular distribution is much wider than for the 1 mm × 1 mm heater shown in Fig. 4.

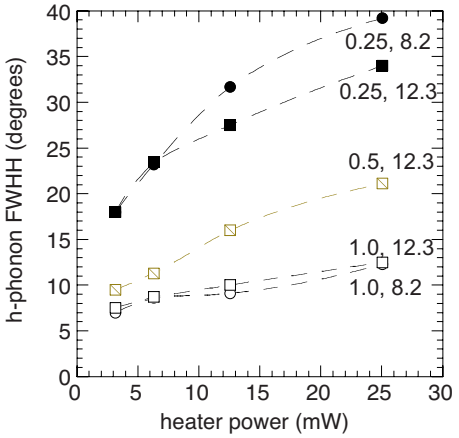

FIG. 7. (Color online) The FWHH of the angular distribution of the time-integrated *h*-phonon signal as a function of heater power for different heaters and distances. The filled circles and squares are for the 0.25 mm heater at 8.2 mm and 12.3 mm, respectively. The open circles and squares are for the 1.0 mm heater at 8.2 mm and 12.3 mm, respectively. The crossed square is for the 0.5 mm heater at 12.3 mm. The random error in the FWHH is ≈1.5° for most points but increases to ≈2.5° for the 1 mm heater at the lowest power. Note that the angular distribution is much wider for the narrow heater.

function of heater power. Also is plotted the results for the heater 0.5 mm wide at a distance of 12.3 mm. It is clear from Fig. 7 that the FWHH increases as the width of the heater decreases, and that it increases with heater power, with a larger increase for the narrower heaters. It appears that the FWHH for the 0.25 mm heater decreases a little with distance between 8.2 and 12.3 mm, at the higher powers, this is probably due to experimental uncertainty.

In Fig. 8, we plot the maximum of the *h*-phonon angular distribution, i.e., at $\theta=0$, as a function of heater power. For most of the power range, the maximum signal for the 0.25 mm heater is not as high as for the 1 mm heater, this is to be expected as if the angular distribution is wider then the height must be lower as the integrated energy must be similar from the two heaters, for the same heater power. However, at the lowest powers the situation is reversed. This is due to the very weak *h*-phonon creation when the heater power *density* is low. It can be seen that there is a soft threshold power density of ≈4 mW mm^{-2}.

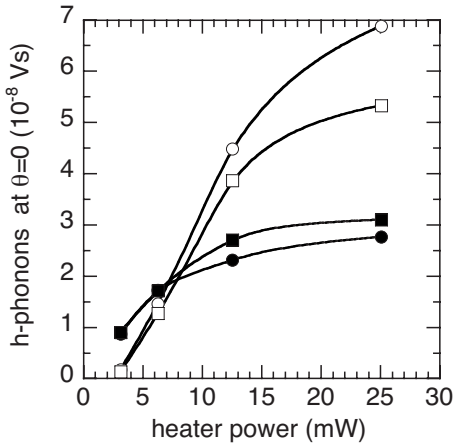

FIG. 8. The time-integrated *h*-phonon signal at $\theta=0$ as a function of heater power. The filled circles and squares are for the 0.25 mm heater at 8.2 mm and 12.3 mm, respectively. The open circles and squares are for the 1.0 mm heater at 8.2 mm and 12.3 mm, respectively. The random error in the signal is indicated by the size of the symbol. Note that there is a soft threshold for *h*-phonon creation of ~4 mW mm^{-2}.

IV. ANALYSIS AND DISCUSSION OF THE RESULTS

The *h*-phonons are mostly created near the heater in the dense pulse of interacting *h*-phonons created by a short heater pulse. Once they are created they fall behind the *l*-phonon pulse and thereafter propagate ballistically to the detector. Near the heater, the *l*-phonon pulse has the lateral dimensions of the heater so the source of *h*-phonons has a similar spatial extent. The *h*-phonon creation rate, at a point in space, depends on the local values of the anisotropy parameters of temperature and velocity. If we suppose that at each point of the source creates *h*-phonons in a cone with a cone angle α, then the lateral extent of the *h*-phonon beam at a distance $d(d \gg h)$ is $2d\alpha+h$, where h is the width of the heater. The corresponding angular width of the *h*-phonon beam is $2\alpha+h/d$. We call the angle 2α the intrinsic angular width of the *h*-phonons which depends on the values of the anisotropy parameters. It is obtained by subtracting h/d from the measured angular width. The correction is most significant for the data from the 1 mm heater because 2α is smallest, as well as h/d being largest for a heater of this size.

The intrinsic angular width of the *h*-phonon distribution in real space is also the angular distribution of *h*-phonon momenta in momentum space because the *h*-phonons propagate ballistically. There is no such connection between the angles in the real and momentum spaces for the *l*-phonons when they are strongly interacting. In momentum space, the angle of the cone of states occupied by the *l*-phonons, increases with heater power.[6] As the three-phonon interaction involves small angles between the phonons, only a fraction of the phonons in the cone interact directly with each other, as discussed in Ref. 7. In real space, the angular distribution of the *l*-phonons is governed by several factors, including the width of the heater, as discussed in Ref. 7.

In Fig. 9, we show the intrinsic FWHH of the *h*-phonons at 12.3 mm, as a function of the reciprocal of the heater width. We see that for each heater power, the data points lie on reasonably straight lines and there is only a weak dependence on heater power, although it is larger than the very weak dependence on power of the mesa width (cf. Fig. 10 in Ref. 7). This dependence on the reciprocal of the heater width is the same as that of the *l*-phonons whose behavior is described by Eq. (1), i.e., the mesa width is inversely proportional to the width of the heater. We take this similarity between *l*- and *h*-phonons as strong evidence that the mesa formation in the angular distribution of the *l*-phonons is directly caused by the creation of *h*-phonons within a few millimeters of the heater. The connection between the two behaviors is due to energy loss from the *l*-phonon system when *h*-phonons are created, and this loss ceasing when the energy

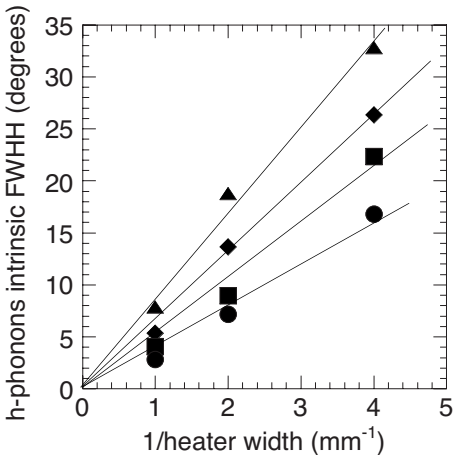

FIG. 9. The intrinsic FWHH of the angular distribution of the time-integrated *h*-phonon signal as a function of the inverse of the heater width, at a heater-bolometer separation of 12.3 mm, for heater powers 3.125 mW (circles), 6.25 mW (squares), 12.5 mW (diamonds), and 25 mW (triangles). The intrinsic FWHH has the geometric effect of the width of the heater removed from the angular distribution, see text. We see that the intrinsic FWHH varies as the inverse of the width of the heater for a given heater power and is only a weak function of heater power.

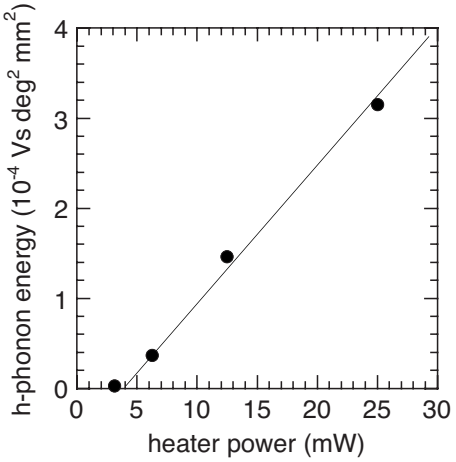

FIG. 10. The total energy in the *h*-phonons (i.e., the *h*-phonon signal integrated over time and angle) as a function of heater power, for the 1×1 mm^2 heater at 12.3 mm. This shows that the total energy in the created *h*-phonons increases linearly with heater power, after a threshold heater power.

density in the *l*-phonons reaches the critical value ε_h over the area of the mesa top. We note that increasing the *l*-phonon energy density in real space by increasing the power to a heater of a given width, has a different effect to increasing the power density by narrowing the width of the heater. This is because the width of the heater determines the energy distribution of the *l*-phonons in real space, as discussed in Ref. 7, and this consequently has an effect on the creation of *h*-phonons

To obtain the total energy in the *h*-phonons, we must integrate the angular emission in three dimensions. As all the *h*-phonons have much the same energy, 10 K, then the bolometer sensitivity can be taken as constant. To obtain the total energy from the signal as a function of angle $S(\theta)$, then one must integrate $2\pi S(\theta)\sin(\theta)$ over θ. However, doing this with noisy data leads to values of the integrals with large uncertainties. This is because the $\sin(\theta)$ function gives more weight to the signals at large θ, and these data have the largest fractional uncertainty. The signals at $\theta\rightarrow0$ have the least uncertainty so it is best to estimate the total energy with these data. As the angular distributions are at small angles to the normal, we adopt the following method: the area of the shell of *h*-phonons at distance *d* is $\pi(d\theta_{1/2}/2)^2$, where $\theta_{1/2}\equiv$FWHH, and we multiply this by the maximum signal $S(\theta=0)$ to obtain an estimate of the total energy in the *h*-phonons. The result of this procedure is shown in Fig. 10, where $(d\theta_{1/2}/2)^2S(\theta=0)$ is plotted against heater power, for the 1 mm at 12.3 mm. Within the large uncertainties, the total energy is the same at 8.2 mm which we would expect as the *h*-phonons are stable once they leave the *l*-phonon pulse. We can only make the integral for the 1×1 mm^2 heater because its angular distribution is reasonably axially symmetric so all the information is in $S(\theta)$. This is not the case for the rectangular-shaped heaters.

Figure 10 shows that the total energy in the *h*-phonons increases linearly with heater power after a threshold power of 4 mW. It is not a trivial result that the total energy in the *h*-phonons increases linearly with heater power. It shows that the heater pulse just increases the initial *number* of interacting *l*-phonons in the helium as power is increased, and does not increase the *l*-phonon energies, i.e., in the Bose-cone model nomenclature, this means that the temperature T_p is constant but the cone angle increases as the heater power increases. This follows from the fact that if T_p were increased then a larger fraction of the *l*-phonons would go to *h*-phonons and so the number of *h*-phonons would increase faster than linearly with heater power. This can be seen with the following argument. Suppose that on increasing the heater power, T_p increased but the cone angle Ω_c remained constant. The energy Q_l in the *l*-phonon system can be written as $Q_l=c\Omega_cT^4$, where *c* is a constant. The energy that goes to the *h*-phonons Q_h is given by $Q_h=Q_{l,i}-Q_{l,f}$, where $Q_{l,i}$ and $Q_{l,f}$ are the initial and final energies of the *l*-phonons, respectively, with corresponding cone angles and temperatures $T_{p,i}$, $\Omega_{c,i}$ and $T_{p,f}$, $\Omega_{c,f}$, respectively. Then Q_h can be expressed as a fraction of the initial energy $Q_{l,i}$ by

$$\frac{Q_h}{Q_{l,i}}=\left(1-\frac{\Omega_{c,f}T_{p,f}^4}{\Omega_{c,i}T_{p,i}^4}\right). \tag{2}$$

Now the supposition is that $\Omega_{c,i}=\Omega_{c,f}$. As the final temperature $T_{p,f}$ is a constant, as it is the temperature at which the *h*-phonons cease to be created, then we see from Eq. (2) that as $T_{p,i}$ increases then $Q_h/Q_{l,i}$ increases. As this is contrary to what is seen experimentally then we must conclude that the supposition is *incorrect* and that $T_{p,i}$ does *not* increase with heater power but the cone angle in momentum space does increase. This confirms the earlier suggestion.[6]

We now turn our attention to compare the *h*-phonons to the *l*-phonons. In Fig. 11, we plot the ratio of the maximum signals, i.e., at $\theta=0$ as a function of heater power *density*, for the 1 mm and 0.25 heaters at the two distances 8.2 mm and

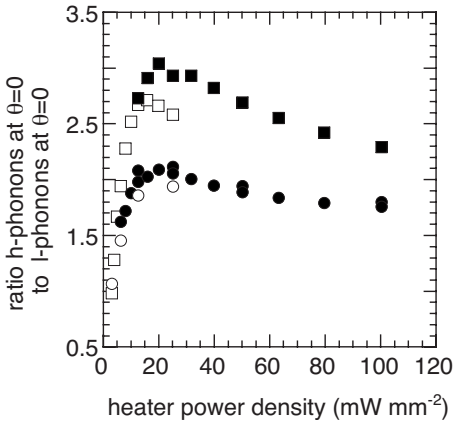

FIG. 11. The ratio of the time-integrated *h*-phonon and *l*-phonon signals at $\theta=0$ as a function of heater power density. The filled circles and squares are for the 0.25 mm heater at 8.2 mm and 12.3 mm, respectively. The open circles and squares are for the 1.0 mm heater at 8.2 mm and 12.3 mm, respectively. We see that when plotted against heater power density, the behavior of the different sized heaters is very similar, at the same distance.

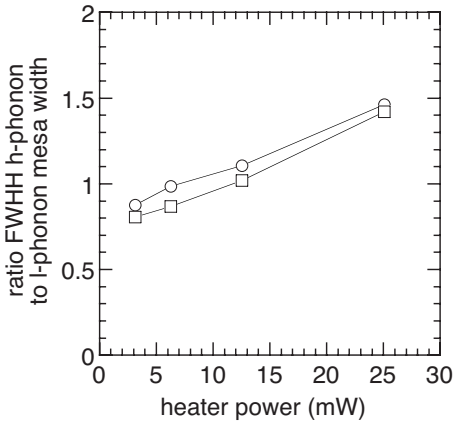

FIG. 12. The ratio of the FWHH of the angular distribution of the *h*-phonons and the width of the mesa of the *l*-phonons, as a function of heater power. The open circles and squares are for the 0.25 mm heater at 8.2 mm and 12.3 mm, respectively. We see the ratio is around 1.

12.3 mm. The *l*-phonon signal is integrated over time as is the *h*-phonon signal. We see that all four curves show the same general shape. The ratio rapidly rises from zero and peaks at around 15 mW mm^{-2} and then slowly decreases. The small values of the ratio at low power densities show that when the *l*-phonon density is very low, very few *h*-phonons are created. However, it is apparent from the figure that initially the *h*-phonon creation rate rapidly increases as it depends strongly on the energy density of the *l*-phonons.[29] The ratio slowly decreases at high-power densities probably due to more scattering of the *h*-phonons within the denser *l*-phonon pulse before they leave it. This scattering within the pulse, by 4pp, reduces the number of *h*-phonons within the pulse and consequently the number that escape the pulse.

From Fig. 11, we see that the ratio is larger at the longer distances. We suggest that this is due to the lateral expansion of the *l*-phonons in real space which causes their energy density to decrease and consequently the phonon spectrum to shift to lower energies. As the bolometer sensitivity decreases with phonon energy, the signal from the *l*-phonons decreases a little, and so the ratio of *h*- to *l*-phonons is higher at the longer distance.

To obtain the ratio of the energy fluxes from the ratio of the signals, we must take into account the different sensitivities of the bolometer to the two groups of phonons. The *l*-phonons have temperature around 0.7 K. For a Bose-Einstein distribution, the average phonon energy is $2.7k_BT$. So for $T=0.7$ K, the average phonon energy is $2k_B$. The *h*-phonons have energy $10k_B$. The bolometer sensitivity rises linearly with energy to a phonon energy of $5k_B$ and is constant at higher energies. So the bolometer is $5/2\times$ more sensitive to the *h*-phonons than to the *l*-phonons. The ratio of the energy fluxes is $2/5\times$ the ratio of the signals shown in Fig. 11. This confirms that the energy fluxes in the *h*-phonons and the *l*-phonons are similar at $\theta=0$.

In Fig. 12, we plot the ratio of the FWHH of the *h*-phonons to the width of the mesa top of the *l*-phonons, both in angular units, for the 0.25 mm heater. There is too much uncertainty in the ratio for the 1 mm heater because of the small values of FWHH of the *h*-phonons and the mesa width, at low powers. We see that the ratio increases slowly with power. This indicates that the width of the *h*-phonon angular distribution increases slightly faster than that of the *l*-phonons as power is increased. This is not inconsistent with the mesa being produced by the creation of *h*-phonons because the *h*-phonons almost stop being created after the pulse has traveled around 4 mm from the heater. It is around this distance that the angular width of the *h*-phonons is similar to the width of the mesa. From that distance, the *h*-phonons travel ballistically and the *h*-phonon width expands geometrically. Meanwhile, the *l*-phonons are still strongly interacting and the experiment suggests that they expand a little more slowly.

In Fig. 13, we plot the ratio of the FWHH of the *h*-phonons to the FWHH of the *l*-phonons. There appears to be a strong correlation between the FWHH of the *h*-phonons and of the *l*-phonons, with the ratio equal to 0.4 for all the heater powers used. This low value reflects the fact that the angular width of the *h*-phonons is much narrower than that of the *l*-phonons. This is consistent with the theory of *h*-phonon creation which showed that *h*-phonons are produced in the central core of the *l*-phonons within a few millimeters of the heater.[5,29]

After the *h*-phonons have stopped being created, the *l*-phonons, propagating near to the heater normal, are cool but still strongly interacting. Any development of the *l*-phonon system which would change the width of the angular distribution and the width of the mesa, can only be due to the effects within the *l*-phonon pulse and does not involve the *h*-phonons. Such possibilities of the lateral expansion of the cool *l*-phonon pulse are analyzed in Ref. 32 and predict a widening of the *l*-phonon mesa width with distance.

V. CONCLUSIONS

We have measured the angular distribution of the *h*-phonons created by a pulse of low-energy phonons, for

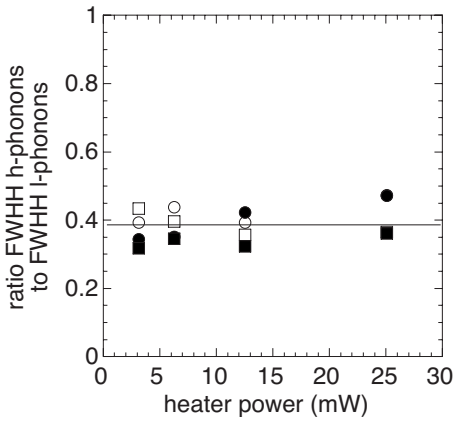

FIG. 13. The ratio of the FWHH of the angular distributions of the *h*-phonons and the *l*-phonons, as a function of heater power. The filled circles and squares are for the 0.25 mm heater at 8.2 mm and 12.3 mm, respectively. The open circles and squares are for the 1.0 mm heater at 8.2 mm and 12.3 mm, respectively. Note that the FWHH of the *l*-phonon angular distribution is ~2.5× that of the *h*-phonons.

three different heater widths, at two distances for a range of heater powers. The distributions are generally narrow but the FWHH of the distributions is larger the narrower the width of the heater. We define a quantity which we call the intrinsic FWHH of the *h*-phonon distributions as the measured FWHH less the extra width due to the geometric effect of the finite width of the heater, i.e., we subtract the angle h/d from the measured angular distribution. We find that the intrinsic FWHH varies inversely with the width of the heater, see Fig. 9. In a previous paper,[7] we reported that the width of the *l*-phonon mesa varied as the reciprocal of the heater width. The fact that both the intrinsic FWHH of the *h*-phonons and the *l*-phonon mesa width have the same dependence on the width of the heater, supports the idea that the formation of the mesa shape in the angular distribution of the *l*-phonons, is due to the creation of *h*-phonons by the *l*-phonons, as was argued in Ref. 7.

We find that there is a clear threshold energy density of the *l*-phonons for the creation of *h*-phonons. It is 4 mW mm^{-2}. The threshold occurs when the creation rate of *h*-phonons becomes negligible at low *l*-phonon energy densities. It is a soft threshold as the *h*-phonon creation rate is low but not zero at low *l*-phonon energy densities. With increasing heater power, both the FWHH of the *h*-phonons and their signal increase. For the smallest width heater, the increase in the FWHH is largest and the signal increase smallest, see Figs. 8 and 9. A very striking result is that the total energy in the *h*-phonons, obtained by integrating over time and angle, is a linear function of heater power. This is shown in Fig. 10 for the 1×1 mm^2 heater. We argue that this is due to the number of *l*-phonons increasing, but not their energy, with heater power.

We have directly compared the behavior of the *l*-phonons and the *h*-phonons. The ratio of the time-integrated *l*- and *h*-phonon signals at $\theta=0$, increases rapidly with heater power *density*, at low heater powers, but reaches an approximate plateau at ~15 mW mm^{-2}. This is shown in Fig. 11. Again the rapid increase shows that the creation rate of the *h*-phonons is a fast function of the *l*-phonon energy density in the liquid helium. We estimate the energy fluxes in *h* and *l*-phonons at $\theta=0$ in the plateau region, taking into account the different responsivities of the bolometer to the two groups of phonons with different energy phonons, and find that the two energy fluxes are about equal. This is a remarkable result when one remembers that the *h*-phonons have been created from the *l*-phonons; it shows that the *h*-phonon creation rate is fast on the scale of the inverse of the propagation time in the experiment.

The ratio of angular widths of the *h*-phonons to the angular width of the *l*-phonons is shown in two ways. The FWHH of the *h*-phonons is compared to the width of the *l*-phonon mesa in Fig. 12, for the 1×1 mm^2 heater and to the FWHH of the *l*-phonons in Fig. 13 for two heaters. The ratio of the FWHH of the *h*-phonons and the width of the *l*-phonon mesa is around 1 but slowly increases with heater power. The FWHH of the *h*-phonons, at a long distance from the heater, increases a little faster than the mesa width because the *h*-phonons are propagating ballistically from their point of creation while the *l*-phonons are propagating as a strongly interacting group, which seems to stop them expanding laterally as fast as the *h*-phonons, at the higher heater powers. The ratio of the FWHH of the *h*- and *l*-phonon angular distributions is independent of heater power and heater width, as can be seen in Fig. 13. At the present, it is not obvious why this is so.

All these results show how the *h* and *l*-phonons are intimately connected and lead to the following picture. The heater injects phonons into liquid helium in non-phonon-energy conserving processes, and the resulting *l*-phonons are strongly interacting at small angles to the normal to the heater. The *l*-phonons create high-energy phonons by 4pp which are left behind by the *l*-phonon pulse soon after creation, and so are left in cold helium which is free of phonons. The *h*-phonons are therefore not scattered and they cannot spontaneously decay so they propagate ballistically to the bolometer. The *l*-phonon pulse loses energy in creating the *h*-phonons and within a few millimeters of the heater, their energy density is so low that *h*-phonon creation is negligible. This causes the angular distribution of the *l*-phonons to form their characteristic mesa shape.

ACKNOWLEDGMENT

We are grateful to I. N. Adamenko for stimulating discussions and helpful comments.

*a.f.g.wyatt@exeter.ac.uk

[1] M. A. H. Tucker and A. F. G. Wyatt, J. Phys.: Condens. Matter **6**, 2813 (1994).
[2] M. A. H. Tucker and A. F. G. Wyatt, J. Low Temp. Phys. **113**, 621 (1998).
[3] I. N. Adamenko, K. E. Nemchenko, A. V. Zhukov, M. A. H. Tucker, and A. F. G. Wyatt, Phys. Rev. Lett. **82**, 1482 (1999).
[4] A. F. G. Wyatt, M. A. H. Tucker, I. N. Adamenko, K. E. Nemchenko, and A. V. Zhukov, Phys. Rev. B **62**, 9402 (2000).
[5] I. N. Adamenko, Y. A. Kitsenko, K. E. Nemchenko, V. A. Slipko, and A. F. G. Wyatt, Phys. Rev. B **73**, 134505 (2006).
[6] R. V. Vovk, C. D. H. Williams, and A. F. G. Wyatt, Phys. Rev. B **68**, 134508 (2003).
[7] D. H. S. Smith and A. F. G. Wyatt, Phys. Rev. B **79**, 144520 (2009).
[8] J. F. Allen and A. D. Misener, Proc. R. Soc. London, Ser. A **172**, 467 (1939).
[9] P. L. Kapitza, J. Phys. (Moscow) **5**, 59 (1941).
[10] P. P. Craig and J. R. Pellam, Phys. Rev. **108**, 1109 (1957).
[11] An example of a quasiequilibrium is a well-mixed bucket of hot water standing in a cooler room. The water can be described by a thermodynamic temperature T which slowly relaxes to room temperature. On time scales short, compared with this relaxation time, the water can be treated as though it were in thermodynamic equilibrium.
[12] I. N. Adamenko, K. E. Nemchenko, V. A. Slipko, and A. F. G. Wyatt, J. Phys.: Condens. Matter **17**, 2859 (2005).
[13] A. F. Andreev and L. A. Melnikovsky, Pis'ma Zh. Eksp. Teor. Fiz. **78**, 1063 (2003) [JETP Lett. **78**, 574 (2003)].
[14] A. F. Andreev and L. A. Melnikovsky, J. Low Temp. Phys. **135**, 411 (2004).
[15] I. N. Adamenko, K. E. Nemchenko, V. A. Slipko, and A. F. G. Wyatt, Phys. Rev. Lett. **96**, 065301 (2006).
[16] I. N. Adamenko, K. E. Nemchenko, V. A. Slipko, and A. F. G. Wyatt, J. Phys.: Condens. Matter **18**, 2805 (2006).
[17] I. N. Adamenko, K. E. Nemchenko, V. A. Slipko, Yu. Kitsenko, and A. F. G. Wyatt, Low Temp. Phys. **31**, 459 (2005).
[18] I. N. Adamenko, Y. A. Kitsenko, K. E. Nemchenko, V. A. Slipko, and A. F. G. Wyatt, Phys. Rev. B **72**, 054507 (2005).
[19] S. Havlin and M. Luban, Phys. Lett. **42A**, 133 (1972).
[20] M. A. H. Tucker and A. F. G. Wyatt, J. Phys.: Condens. Matter **4**, 7745 (1992).
[21] I. N. Adamenko, Yu. A. Kitsenko, K. E. Nemchenko, and A. F. G. Wyatt, Fiz. Nizk. Temp. **35**, 265 (2009).
[22] I. N. Adamenko, K. E. Nemchenko, and A. F. G. Wyatt, Low Temp. Phys. **29**, 11 (2003).
[23] I. M. Khalatnikov, *An Introduction to the Theory of Superfluidity* (Addison-Wesley, Redwood City, CA, 1989).
[24] H. J. Maris and W. E. Massey, Phys. Rev. Lett. **25**, 220 (1970).
[25] J. Jäckle and K. W. Kehr, Phys. Rev. Lett. **27**, 654 (1971).
[26] R. A. Sherlock, N. G. Mills, and A. F. G. Wyatt, J. Phys. C **8**, 2575 (1975).
[27] A. F. G. Wyatt, N. A. Lockerbie, and R. A. Sherlock, Phys. Rev. Lett. **33**, 1425 (1974).
[28] R. C. Dynes and V. Narayanamurti, Phys. Rev. Lett. **33**, 1195 (1974).
[29] I. N. Adamenko, K. E. Nemchenko, V. A. Slipko, Yu. A. Kitsenko, and A. F. G. Wyatt, Low Temp. Phys. **33**, 387 (2007).
[30] T. W. Bradshaw and A. F. G. Wyatt, J. Phys. C **16**, 651 (1983).
[31] D. H. S. Smith and A. F. G. Wyatt, Phys. Rev. B **76**, 224519 (2007).
[32] I. N. Adamenko, K. E. Nemchenko, and V. A. Slipko, J. Low Temp. Phys. **159**, 492 (2010).
[33] R. A. Sherlock and A. F. G. Wyatt, J. Phys. E **16**, 673 (1983).
[34] R. A. Sherlock, J. Phys. E **17**, 386 (1984).
[35] C. D. H. Williams, Meas. Sci. Technol. **1**, 322 (1990).
[36] D. H. S. Smith, R. V. Vovk, C. D. H. Williams, and A. F. G. Wyatt, New J. Phys. **8**, 128 (2006).
[37] P. C. Hendry and P. V. E. McClintock, Cryogenics **27**, 131 (1987).